Stable, Covalent Attachment of Laminin to Microposts Improves the Contractility of Mouse Neonatal Cardiomyocytes

Alexandre J. S. Ribeiro,[†,‡] Kathia Zaleta-Rivera,[‡,||] Euan A. Ashley,[‡,||] and Beth L. Pruitt*[,†,‡]

[†]Department of Mechanical Engineering and [‡]Stanford Cardiovascular Institute, Stanford University, Stanford, California United States

[||]Department of Cardiovascular Medicine, Stanford University School of Medicine, Stanford, California United States

S *Supporting Information*

ABSTRACT: The mechanical output of contracting cardiomyocytes, the muscle cells of the heart, relates to healthy and disease states of the heart. Culturing cardiomyocytes on arrays of elastomeric microposts can enable inexpensive and high-throughput studies of heart disease at the single-cell level. However, cardiomyocytes weakly adhere to these microposts, which limits the possibility of using biomechanical assays of single cardiomyocytes to study heart disease. We hypothesized that a stable covalent attachment of laminin to the surface of microposts improves cardiomyocyte contractility. We cultured cells on polydimethylsiloxane microposts with laminin covalently bonded with the organosilanes 3-glycidoxypropyltrimethoxysilane and 3-aminopropyltriethoxysilane with glutaraldehyde. We measured displacement of microposts induced by the contractility of mouse neonatal cardiomyocytes, which attach better than mature cardiomyocytes to substrates. We observed time-dependent changes in contractile parameters such as micropost deformation, contractility rates, contraction and relaxation speeds, and the times of contractions. These parameters were affected by the density of laminin on microposts and by the stability of laminin binding to micropost surfaces. Organosilane-mediated binding resulted in higher laminin surface density and laminin binding stability. 3-glycidoxypropyltrimethoxysilane provided the highest laminin density but did not provide stable protein binding with time. Higher surface protein binding stability and strength were observed with 3-aminopropyltriethoxysilane with glutaraldehyde. In cultured cardiomyocytes, contractility rate, contraction speeds, and contraction time increased with higher laminin stability. Given these variations in contractile function, we conclude that binding of laminin to microposts via 3-aminopropyltriethoxysilane with glutaraldehyde improves contractility observed by an increase in beating rate and contraction speed as it occurs during the postnatal maturation of cardiomyocytes. This approach is promising for future studies to mimic *in vivo* tissue environments.

KEYWORDS: *3-glycidoxypropyltrimethoxysilane, 3-aminopropyltriethoxysilane, glutaraldehyde, neonatal cardiomyocytes, poly(dimethylsiloxane) microposts, surface functionalization, contractility*
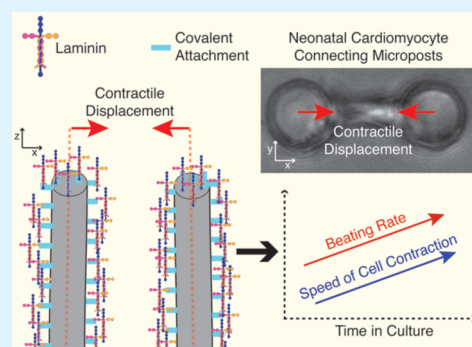
1. INTRODUCTION

Heart disease is the main cause of death in developed nations[1] and presents a heavy financial burden on public and private spending.[1] Abnormal heart mechanical output is indicative of failure and disease.[2] The profile of cell shortening[3] and force generation[4] in the contractility of single cardiomyocytes, the muscle cells of the heart, has been related to pathophysiological properties.[5] However, the roles of single-cell contractility and of the extracellular factors that control it are still poorly understood. Changes in the composition and morphology of the extracellular matrix that occur during heart development[6] and heart disease[7] affect the activity of cardiomyocytes.[8] Therefore, systems that can simultaneously measure cell-generated forces and expose cells to tunable extracellular composition are needed to study biomechanical phenotypes.

Culturing cardiomyocytes on polydimethylsiloxane (PDMS) micropost arrays can enable a simple and inexpensive assay of force generation[9,10] that offers the potential for high-

throughput investigations of myocardial health based on single-cell *mechanobiology*. Other methods have been developed to measure the forces generated by contractile cardiomyocytes, such as atomic force microscopy,[11] micropipette aspiration,[12] and carbon fibers/glass rods connected to piezoelectric actuators.[4] These techniques are not readily scalable for high-throughput investigations and require skilled technical expertise, limiting their potential for biological studies.

Murine cardiomyocytes have been used for decades in the study of cardiac biology at the single-cell level,[13] but the use of these cells in single-cell mechanobiology studies is limited by their low adhesion to common culture substrate materials.[14] Here we used single neonatal cardiomyocytes (neoCMs) because they can be cultured for longer times and have been

ACS Publications
15516
dx.doi.org/10.1021/am5042324 | ACS Appl. Mater. Interfaces 2014, 6, 15516−15526

extensively used as models to study cardiomyocyte mechanobiology.[15] The role of the adhesion of the extracellular matrix to PDMS microposts in neoCM mechanobiology has not been reported. The efficiency of neoCM adhesion to microposts functionalized with physisorbed cellular adhesive proteins after oxidation is low.[10] We hypothesized that a more stable attachment of extracellular matrix proteins to the surface of microposts will improve adhesion and affect the biomechanical activity of neoCMs. For example, the availability, attachment, and density of cell ligands on the substrate surface affect the mechanobiology of other types of adhesive cells.[16−18]

NeoCMs are usually cultured on laminin-coated substrates.[19] *In vivo*, laminin physically connects cardiomyocytes to the connective tissue[20] and mediates the internalization of extracellular mechanical cues.[21] Laminin in the myocardium is mainly present in the basement membrane in direct contact with cardiomyocytes, and it is one of its major components.[22] Cytoskeletal organization in muscle cells[23] and *in vitro* myogenic activity of skeletal muscle tissue constructs[24] also vary with the quantity of extracellular laminin.

Here we aim to show a relation between the strength of laminin binding to the surface of microposts and the contractile phenotypes of neoCMs. We covalently linked laminin to PDMS microposts, analyzed the stability of laminin attachment, and characterized micropost deflections during the contraction of immobilized neoCMs. The organosilanes 3-glycidoxypropyltrimethoxysilane (GPTMS)[25] and 3-aminopropyltriethoxysilane with glutaraldehyde (APTES^{glut})[26] were bonded to oxidized microposts to covalently link laminin to the surface. These compounds have already been used to bind biomolecules to PDMS and improve adhesion of other cell types.[18]

2. EXPERIMENTAL SECTION

2.1. Fabrication of Elastomeric Micropost Arrays. We used PDMS microposts (20 μm in diameter and 90 μm in height) to measure the force generated by contractile neoCMs (Figure 1). We fabricated arrays of microposts from transparency masks following established soft-lithography techniques using PDMS double molding from similar posts of SU-8 negative photoresist on a silicon wafer (Figure 1).[9] Unless indicated otherwise, we purchased SU-8 and SU-8 related materials from Microchem (Newton, MA, USA), we purchased PDMS from Dow Corning (Midland, MI, USA), and we purchased other chemical substances from Sigma-Aldrich (St. Louis, MO, USA). We used a 10 μm base layer of SU-8 beneath the SU-8 microposts to promote adhesion to silicon wafers (mechanical grade, University Wafer, Boston, MA, USA). We spin-coated SU-8 negative photoresist (SU-8 3010) on wafers for 30 s at 3500 rpm. We baked the SU-8 on a hot plate (ramp from 65 to 95 °C and held for 6.5 min). We exposed the wafer to ultraviolet light for 8.5 s at 20 mW/cm^2 (OAI, San Jose, CA, USA; light source centered at 365 nm) through a high-pass ultraviolet filter (PL-360-LP, Omega Optical, Brattleboro, VT, USA) and postbaked the SU-8 (ramp from 65 to 95 °C and held for 2.5 min). We dried the wafer with N$_2$ gas after developing the SU-8 for 4.5 min with SU-8 developer.

For the fabrication of microposts (Figure 1), we spin-coated another type of SU-8 (SU-8 2050) to form a 90 μm thick layer on the precoated wafer for 30 s at 1750 rpm and baked the SU-8 for 5 min at 65 °C and 15 min at 95 °C before ultraviolet-light exposure with a transparency mask as described above for 12 s (FineLine Imaging, Colorado Springs, CO, USA). We did postexposure baking for 5 min at 65 °C and for 9.5 min at 95 °C. After each baking step, wafers were placed on a hot plate at 65 °C for 5 min and stored for 20 min at room temperature to promote slower cooling. We developed uncured SU-8 as previously described for 9 min. After the wafers were developed and dried with N$_2$ gas, we exposed the wafers at room temperature and atmospheric pressure in chlorotrimethylsilane for 3 h to minimize SU-
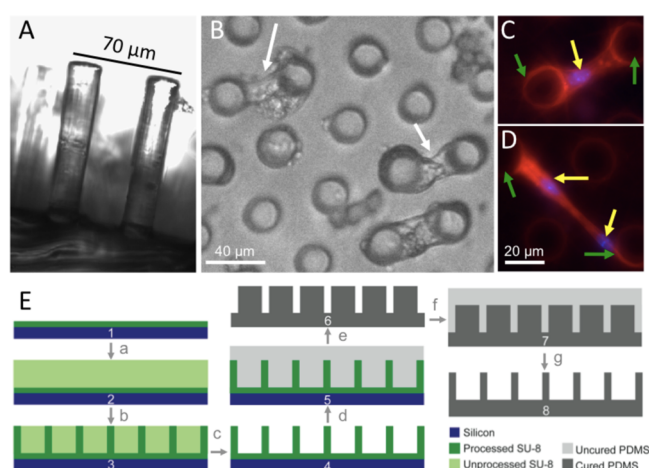
Figure 1. Elastomeric PDMS micropost arrays for sensing force generated by attached neoCMs. (A) Cross-sectional view of adjacent microposts 20 μm in diameter and 100 μm in height. (B) Top view of micropost arrays with immobilized, live, beating neoCMs (white arrows). (C, D) Fixed neoCMs immobilized between microposts with labeled actin (red) and nuclei (blue). Single neoCMs attach between adjacent microposts (C). Cell-based connections between nonadjacent microposts involve more than one neoCM and were not used for analysis (D). The yellow arrows point the number of cells. The green arrows denote the microposts to which cells are attached. (E) Method for fabricating micropost arrays via soft lithography and PDMS double molding.

8 adhesion to PDMS during molding. We mixed PDMS-184 (Sylgard 184) prepolymer and curing agent in a 10:1 ratio (Thinky, Laguna Hills, CA, USA), cast uncured PDMS-184 on the wafer and cured it for 24 h at 70 °C. We then carefully peeled back the PDMS-184 molds. To facilitate the release of final PDMS structures from the mold, we plasma-treated molds at 66.6 Pa and 80 W in an oxygen plasma asher (Branson IPC/Novellus, San Jose, CA, USA) for 10 s and silanized as described above for 24 h. We cast-mixed 10:1 PDMS−182 (Sylgard 182) on the molds and degassed before curing at 70 °C for 24 h. We obtained micropost arrays by peeling the cured PDMS surface from the PDMS−184 molds.

2.2. Covalent Attachment of Laminin to PDMS. We autoclaved all fabricated arrays to sterilize them before any surface modification. We diluted laminin-111 isolated from mice (BD Biosciences, San Jose, CA, USA) in phosphate-buffered saline (PBS; pH 7.2) (for GPTMS) or Milli-Q water (for APTES^{glut}) to a concentration of 10 μg/mL. We bound organosilanes[27] under sterile conditions to oxidized PDMS surfaces to promote covalent cross-linking of laminin to the surfaces of the microposts (Supporting Information, Figure S1). We oxidized PDMS micropost arrays with plasma for 20 s as previously described and incubated them for 1 h under anoxic conditions in an anhydrous methanol solution of 20% GPTMS or 5% APTES with 0.005% acetic acid. These concentrations have been shown to generate self-assembled monolayers of organosilanes on silica-based flat surfaces.[28] The silanized arrays were washed three times with methanol and three times with Milli-Q water. We further incubated APTES functionalized surfaces for 30 min in a solution of 1% glutaraldehyde (Electron Microscopy Sciences, Hatfield, PA, USA) in Milli-Q water and washed them three times with Milli-Q water to functionalize surfaces with APTES^{glut}. We incubated micropost arrays in laminin-111 solution for 2 h. Substrates were incubated three times in PBS (pH 7.2) to wash away unattached laminin.

2.3. Isolation and Culture of Mouse neoCMs. Unless indicated otherwise, we purchased all cell-culture components from Life Technologies (Grand Island, NY, USA). We isolated neoCMs from neonatal mice aged 3 d as previously described.[29] The administrative panel on laboratory animal care (APLAC) from Stanford University approved all the protocols for mice neonatal heart isolation. We

sacrificed 10−12 pups for each test. We performed two tests with neoCMs in this work. We used a mix of male and female because it is hard to quickly assess gender in newborn mice. In summary, we put CD-1 strain mice (white mice originated from the caesarean derivation (CD) of a non-inbred Swiss albino mouse in 1959) to sleep with mild hypothermia for sacrifice. The hearts were excised and rapidly transferred into ice-cold calcium- and bicarbonate-free Hanks with Hepes (CBFHH) buffer. We placed the hearts in a solution of papain (Papain Dissociation System, Worthington Biochemical Corporation, Lakewood, NJ, USA) in 10 mL of CBFHH and digested them for 30 min at 37 °C with mild shaking and gentle pipetting. We collected cells in a tube containing fetal bovine serum (100X) by filtering the solution through a nylon mesh and centrifuging the tube at 1000 rpm for 20 min. The resulting cells were suspended in 10 mL of neonatal mouse medium (1X Dulbecco's Modified Eagle Medium containing 5% fetal bovine serum, 10% horse serum, penicillin (25 μg/mL), and streptomycin (50 μg/mL)) and were transferred to an untreated Petri dish. We incubated the cells for 1 h at 37 °C in 5% CO_2 to allow fibroblast attachment. We collected and suspended the nonattached neoCMs in neonatal mouse medium containing 1 μM cytosine-β-D-arabinofuranoside to inhibit the proliferation of contaminating nonmyogenic cells.

2.4. Microscopy, Video Acquisition, and Fluorescent Labeling. We imaged neoCMs and devices using an inverted microscope (Leica Microsystems, Buffalo Grove, IL, USA) with an environmental chamber, fluorescence capabilities, and an automated stage, which allows for quantification of heights. We acquired videos (as presented in the Supporting Information, Video) and images with a CCD camera (Orca-R2, Hamamatsu, Bridgewater, NJ, USA) and MetaMorph NX2.0 software (Molecular Devices, Sunnyvale, CA, USA). We determined dimensions of images in video frames (Figure 1 and Supporting Information, Figure S2) using a calibration slide (Electron Microscopy Sciences, Hatfield, PA, USA). Prior to fluorescence labeling (Figures 1C,D and 2), we fixed cells with 4% paraformalde-
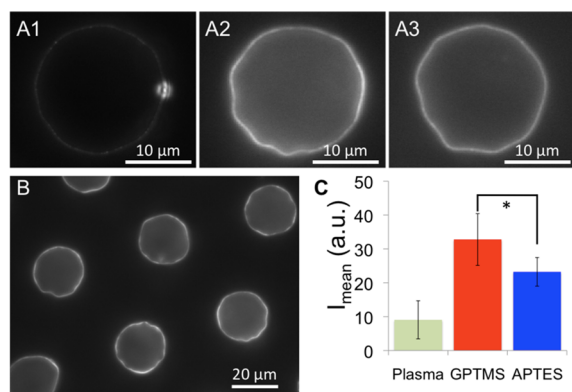
Figure 2. Fluorescent labeling via ICC of laminin on microposts after functionalization. (A) Images of the top surfaces of individual posts where laminin was (A1) physisorbed after plasma treatment, (A2) covalently attached with GPTMS, and (A3) covalently attached with APTES[glut]. (B) Representative fluorescence image of arrays of microposts with labeled laminin covalently attached to the surface with GPTMS. (C) Quantification of mean fluorescence intensity on micropost surfaces. APTES represents APTES[glut]. Intensities were calculated for 20 surfaces and averaged. *p < 0.001 by two-sided Student's t-test. ANOVA p-value < 0.001. Error bars represent the standard deviation of the mean.

hyde (Electron Microscopy Sciences) in PBS for 15 min, permeabilized in 0.1% Triton X-100 (Fisher Scientific, Houston, TX, USA) in PBS for 20 min, and blocked in 2% bovine serum albumin (BSA). To stain actin (Figure 1C,D), we incubated fixed neoCMs for 30 min in a solution of rhodamine phalloidin (VWR, San Dimas, CA, USA) diluted 40 times in 0.2% BSA in PBS. We labeled nuclei by incubating cells in 1 μg/mL 4′,6-diamidino-2-phenylindole in PBS.

Samples were washed three times with PBS between steps. We mounted stained samples on glass with ProLong Gold Antifade Reagent (Life Technologies) and sealed them with clear nail polish.

To label laminin on arrays of functionalized microposts, we used immunocytochemistry (ICC) with mouse primary antilaminin antibody (Life Technologies) at a 1:100 dilution in 0.2% BSA solution in PBS after fixation in paraformaldehyde and incubation in 2% BSA. Before mounting samples, we incubated laminin-tagged microposts for 45 min in 10 μg/mL of Alexa Fluor 488 Goat antimouse antibody (Life Technologies) with 0.2% BSA solution in PBS for fluorescence labeling. Oregon Green 488 conjugated gelatin from pig skin (Life Technologies) was also covalently bound to micropost surfaces as described for laminin. For fluorescently labeled microposts, we quantified the mean fluorescence intensity on the tops of the microposts (excluding the edges) from microscope images with ImageJ 1.43u (NIH, Bethesda, MD, USA). We acquired images at constant optical and acquisition hardware and software parameters. We created a duplicate for each image and removed the edges of posts. We converted these images to binary images to get regions of interest and calculate post intensities in the original images.

2.5. Calculation of Micropost Deflections (δ_t) from Videos of Immobilized neoCMs. We acquired videos (Supporting Information, Video S1) of beating neoCMs immobilized between microposts at frame rates >45 fps with bright-field microscopy, focusing on the tops of the microposts for a maximum time of 10 s. Video postprocessing was performed with ImageJ (Supporting Information, Figure S2). We converted the video frames to eight-bit files and applied a threshold to obtain a dark background and dark post centers surrounded by a white region of invariable morphology. We isolated the tops of the microposts from the dark background by using a duplicate for each frame with an erased micropost region that we subtracted from the original frames. We tracked micropost position across frames with an ImageJ (NIH) multitracker plug-in,[30] which can determine the micropost position within the frame with Cartesian coordinates x_i and y_i. We calculated the distance in pixels of the center of microposts from the origin ($p_i = (x_i^2 + y_i^2)^{1/2}$) for each frame i. We calculated micropost deflection (δ_t) by subtracting the minimum of p_i (p_0, no contractility) from $p_i(t)$ values. Pixel values were converted to μm from measurements with microscopy calibration. The time for each frame was calculated by dividing the frame number by the frame rate.

2.6. Calculation of Functional Parameters to Evaluate the Mechanobiology of neoCMs. For each video of contractile neoCMs, we extracted the maximum post deflection (δ_{max}) from the micropost deflection curves (Figure 3 and Supporting Information, Figure S2). The effective frequency (f^*) measures the contractility rate and was calculated from the average number of wave peaks per second in the 8−10 s deflection curve of each neoCM. Other CM biomechanical functionality parameters were also calculated:

$$V^*_{c\,max} = \frac{VC_{max}}{\delta_{max}} \qquad (eq\ 1)$$

$$V^*_{r\,max} = \frac{VR_{max}}{\delta_{max}} \qquad (eq\ 2)$$

$$t_{CR} = t(VR_{max}) - t(VC_{max}) \qquad (eq\ 3)$$

$V^*_{c\,max}$ and $V^*_{r\,max}$ represent the normalized maximum velocities of contraction and relaxation, respectively, calculated by dividing the maximum velocity of contraction (VC_{max}) or relaxation (VR_{max}; Figure 3) by the maximum deflection (δ_{max}) of the microposts for each cell beat. The time between the time at which relaxation velocity is maximum and the time at which contraction velocity is maximum (t_{CR}) is calculated by subtracting the time of VC_{max} from the time of VR_{max} and is proportional to the time of individual beats.

2.7. Characterization of Surface Chemistry, Stability, and Affinity to Proteins. We semiquantified available amine groups ($-NH_2$) on the surface of APTES-PDMS with ninhydrin (Sigma-Aldrich; Supporting Information, Figures S3 and S4). We incubated surfaces in 1 mg/mL ninhydrin in ethanol for 1 h, washed with Milli-Q
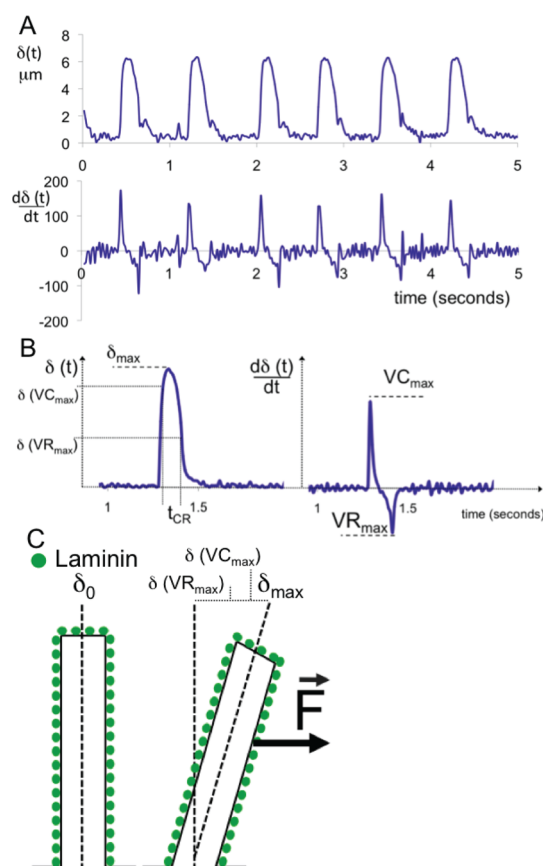
Figure 3. Parameters measured to evaluate single contractions of immobilized neoCMs. (A) Micropost velocity ($d\delta/dt$) is calculated from the central derivative of micropost deflections (δ) with time. (B) Detail of a single contraction curve. For each curve, we determined the following parameters to evaluate contractility: maximum deflection (δ_{max}), maximum velocity of contraction (VC_{max}), maximum velocity of relaxation (VR_{max}), and the difference between the times of VR_{max} and VC_{max} (t_{CR}), which is based on micropost deformation. (C) Representation of the relationship between the measured parameters and the deflection of single microposts. Deformation of the post schematic is approximate; see ref 9 for detailed discussion of micropost deformation.

water, and dried under a gas stream of N_2 before measuring the surface absorption of light at 570 nm with ultraviolet−visible absorption spectroscopy (UV 1800 Spectrophotometer, Shimadzu Scientific Instruments, Columbia, MD, USA).[31] Absorption was then measured for anhydrous solutions with varying concentrations of APTES in methanol and 1 mg/mL ninhydrin to generate calibration curves relating concentration of NH_2 to absorption. We converted absorbance to (C_{eq}) through a calibration curve (Supporting Information, Figure S4B) calculated from the linear regression of absorbance measurements at 570 nm of anhydrous APTES solutions with ninhydrin at set concentrations. We also semiquantified the presence of surface amine-reactive species, such as the glycidoxy group in GTPMS or the aldehyde group in APTES[glut], with toluidine blue O (Sigma-Aldrich; Supporting Information, Figures S3 and S5). We incubated surfaces in 10 mM of NaOH in Milli-Q water for 1 h, washed with Milli-Q water, and dried with N_2 gas. Absorption measurements were performed at 660 nm,[32] and calibration was done with different solutions of toluidine. We calculated toluidine blue O C_{eq} from the surface absorbance of 660 nm, and generated a calibration curve from absorbance measurements of known concentrations of toluidine blue O solutions. We also submitted clean and dried surfaces to contact-angle analysis (Supporting Information,

Figure S6) (FTA 1000, First Ten Angstroms, Portsmouth, VA, USA) with deionized water to measure wettability.

2.8. Statistical Analysis. Unless indicated otherwise, we analyzed statistical differences between means of populations with the Wilcoxon−Mann−Whitney rank sum test for unpaired data,[33] which quantifies statistical differences when populations are not normally distributed. For noted populations with a normal distribution, we also used two-sided Student's t-test[33] to evaluate statistical differences between two populations and ANOVA (analysis of variance)[33] to test statistical differences within three populations.

3. RESULTS

3.1. Protein Density and Stability on Functionalized Substrates Varies with the Type of Organosilane. We cultured cells on PDMS microposts with covalently attached laminin via GPTMS (GPTMS[laminin]) and APTES-glutaraldehyde (APTES[glut-laminin]) (Table 1). We first tested if these two

Table 1. Acronyms for the Different Levels of PDMS Organosilane-Mediated Functionalizations Detailed in Supplementary Information, Figure S1

surface treatment	modified micropost PDMS surface	
organosilane	GPTMS	APTES
glutaraldehyde		APTES[glut]
laminin	GPTMS[laminin]	APTES[glut-laminin]

methods yield microposts surfaces with the same density of attached protein and similar binding stability. We later cultured neoCMs on micropost devices functionalized with GPTMS[laminin] and on microposts functionalized with APTES[glut-laminin] to analyze their contractile phenotypes. We utilized four assessments of protein binding to analyze the efficiency of the methods to bind laminin to PDMS and to minimize the uncertainty associated with any of each assessment. We initially performed ICC against laminin to assay the amount of laminin on the microposts. We then examined the binding of a different protein, fluorescently tagged gelatin, to the microposts. Gelatin is an extracellular matrix component used *in vitro* for culture of cardiomyocytes.[13] The stability of the surface chemistry over time was assessed via contact-angle analysis. Lastly, two colorimetric assays were employed to evaluate the ability of the organosilane functionalized surfaces to bind proteins and ligands.

Microposts were ICC labeled for laminin after functionalization to test differences in laminin levels between different methods of laminin functionalization. We used laminin physisorbed to plasma treated PDMS as a control. Signal intensity and surface coverage were higher on posts with covalently attached laminin (Figure 2A). We analyzed laminin intensity on the top surface of the microposts (Figure 2B). Mean fluorescence intensity was more than three times higher for GPTMS[laminin] posts ($I_{mean} = 32.8 \pm 7.6$ au) than for plasma-treated posts ($I_{mean} = 9.0 \pm 5.6$ au; Figure 2C). Higher amounts of laminin were detected on the surface of GPTMS posts ($I_{mean} = 32.7 \pm 7.6$ au) than on APTES[glut] posts ($I_{mean} = 23.2 \pm 4.2$ au; Figure 2C), suggesting the existence of higher protein surface density on GPTMS treated microposts

We used fluorescently conjugated gelatin to measure protein binding to organosilanes as an alternative to ICC staining and as a control of observed results. Nonspecific binding of fluorophores and antibodies can affect the quantification of protein levels with ICC.[34] The intensity of fluorescently conjugated gelatin scales with protein amount while avoiding

15519

dx.doi.org/10.1021/am5042324 | *ACS Appl. Mater. Interfaces* 2014, 6, 15516−15526

noncontrollable, nonspecific interactions.[35] Fluorescently tagged gelatin was covalently attached to microposts, as performed with laminin (Supporting Information, Figure S1), and the fluorescence intensities on the tops of posts were also measured (Figure S7). As with ICC-labeled laminin, higher fluorescence was detected on GPTMS[gelatin] (62.7 ± 3.3 au) than on APTES[glut-gelatin] posts (34.4 ± 1.5 au; $p < 0.001$) (Supporting Information, Figure S7B).

The purpose of these tests is to evaluate the stability of laminin attachment to surfaces with the different functionalizations. In aqueous environments, the binding of laminin with organosilanes to PDMS surfaces may be degraded due to hydrolysis,[36] possibly affecting the cell-laminin interface over time. In addition, a portion of the observed labeled proteins may interact with surfaces via noncovalent intermolecular interactions with proteins stably attached to the PDMS surface. We sonicated the micropost arrays in PBS to induce removal of noncovalently attached protein from the surface and test these hypotheses. GPTMS[gelatin] microposts showed greater protein loss than APTES[glut-gelatin] microposts after sonication (Supporting Information, Figure S7C), indicating that the binding of detected proteins to APTES[glut] surfaces is more stable. However, compared to physisorption, higher protein amounts are observed in organosilane-functionalized PDMS. Sonication of arrays of microposts with physisorbed fluorescently conjugated gelatin resulted in higher, but not complete, loss of protein from the tops of the microposts (Supporting Information, Figure S7C).

To further test the stability of organosilane functionalization with time, contact-angle analysis was carried out on 10 different dried and clean regions of GPTMS and APTES surfaces (Supporting Information, Figure S6). Measurements were performed directly after surface functionalization (day 0) and after 2 d of incubation in water or anhydrous methanol. Right after functionalization on day 0, the average contact angles of GPTMS and APTES surfaces were $107.4 \pm 0.1°$ and $97.4 \pm 1.7°$, respectively ($p < 0.002$). After 2 d in Milli-Q water, the average contact angles of GPTMS and APTES surfaces were $67.8 \pm 3.3°$ and $100.6 \pm 0.4°$ ($p < 0.005$), respectively, while these angles were $99.9 \pm 5.7°$ and $102.1 \pm 1.1°$ ($p > 0.05$), respectively, after 2 d in anhydrous methanol (Supporting Information, Figure S6). The contact angle of APTES surfaces did not significantly vary after incubation in any of the tested liquids. Unmodified PDMS has a contact angle of ~100° that does not vary with time.[37]

The binding ability of the functionalized material to amines in proteins was determined by colorimetric analysis with toluidine blue O (Supporting Information, Figure S3). The amine functionality of the dye was bound to GPTMS/APTES-glut using the same process that occurs during protein binding. GPTMS or APTES[glut] bind amines exposed on the protein surface (Supporting Information, Figure S1). GPTMS contains a glycidoxy group that directly binds amines, while APTES contains an amine group that is cross-linked to available amines with glutaraldehyde (Supporting Information, Figure S1) (APTES[glut]). APTES[glut], GPTMS and O_2 treated PDMS surfaces were labeled with toluidine blue O. The density of surface-bonded dye molecules was semiquantified via ultraviolet–visible absorbance spectroscopy (Supporting Information, Figure S5). We used plasma-treated PDMS as a blank surface to measure the absorbance of GPTMS surfaces and APTES[glut] surfaces, which generated a residual toluidine signal (Supporting Information, Figure S5A). GPTMS surfaces

presented higher equivalent concentration (C_{eq}) ($C_{eq} = (3.3 \pm 0.6) \times 10^{16}$ particles/mL) and therefore higher amine-bonding potential than APTES[glut] ($C_{eq} = (1.7 \pm 0.6) \times 10^{16}$ particles/mL) (Supporting Information, Figure S5) ($p < 0.0001$). These data suggest that GPTMS surfaces are capable of binding more laminin than APTES[glut] surfaces, which is consistent with our observations in the fluorescent assays.

APTES and APTES[glut] covalent binding to PDMS surfaces was additionally tested with a ninhydrin-based colorimetric assay (Supporting Information, Figure S3) that detects the presence of amines. Nonplasma-treated PDMS surfaces preincubated in APTES and plasma-treated PDMS surfaces with GPTMS, APTES, and APTES[glut] were tested (Supporting Information, Figure S4). A stronger signal was qualitatively observed on the surface of APTES PDMS (Supporting Information, Figure S4A), indicating higher levels of amines on this surface. Quantification of amines was further performed with absorbance measurements at 660 nm of APTES-incubated PDMS surfaces after plasma treatment and incubated without plasma treatment (PDMS). On average, C_{eq} was three times higher on APTES plasma-treated surfaces ($(23.8 \pm 8.3) \times 10^{16}$ particles/mL) than on APTES nonplasma-treated surfaces ($(8.1 \pm 5.8) \times 10^{16}$ particles/mL) (Supporting Information, Figure S4C), indicating that amine density was higher on this surface ($p < 0.0001$).

3.2. Covalent Attachment of Laminin via GPTMS Increases Displacement and Contraction Velocity in neoCMs. Laminin was covalently bound (Supporting Information, Figure S1) to microposts to analyze the effects of enhanced cell adhesion on the contractility of cardiomyocytes. Control surfaces were functionalized according to previously used methods for neoCM adhesion[9] in which laminin is incubated and physisorbed onto PDMS oxidized with oxygen plasma. Since our microposts have the same material and dimensions, we use micropost displacement for relative comparison of contractile phenotypes between cells. Independent of the strategy for laminin surface functionalization, neoCMs attached to the sides of the microposts (Figure 1B) at an average height of 52 ± 15 μm ($n = 15$), which was calculated from the height of cell focal planes to the focal planes of the tops of the microposts.

For each test, neoCMs were simultaneously isolated and different devices were fabricated in parallel to avoid noncontrollable variability in results associated with differences in cell isolation and fabrication materials and conditions. We only analyzed singles cells, which connect two adjacent microposts. At least two cells are necessary to interconnect nonadjacent microposts and we did not analyze these cases (Figure 1D).

In an initial set of tests, neoCMs were cultured on micropost arrays with laminin covalently attached via GPTMS and on arrays with laminin physisorbed through incubation after plasma treatment. Cell attachment to microposts with physisorbed laminin on plasma-treated surfaces was possible after a minimum laminin incubation time of 12 h.

Videos were acquired on the second day after the neoCMs started to beat (Supporting Information, Video S1), typically 4–6 d after plating. Microposts with physisorbed laminin deflected less ($\delta_{max} = 4.1 \pm 0.4$ μm) than microposts where laminin was covalently bound ($\delta_{max} = 8.8 \pm 2.2$ μm; $p < 0.04$; Figure 4A). We observed no difference in effective frequency (f^*) between laminin-physisorbed microposts ($f^* = 3.1 \pm 0.4$ s^{-1}) and microposts with covalently attached laminin ($f^* = 3.0 \pm 0.5$ s^{-1}; Figure 4B). The normalized maximum velocity of
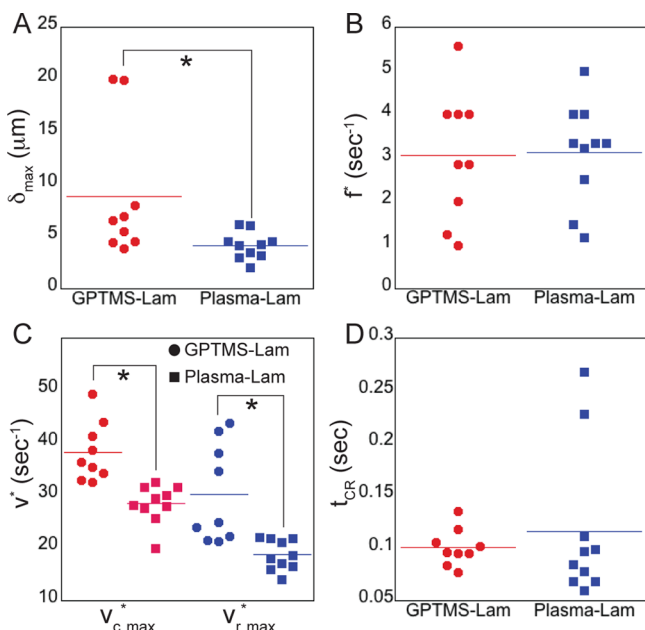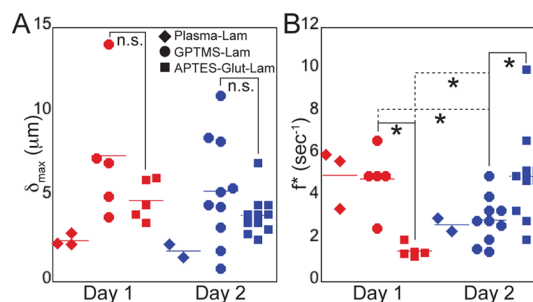
Figure 4. Contractility parameters of neoCMs cultured on micropost arrays with laminin covalently attached to the surface with GPTMS (GPTMS-Lam) ($n = 9$) or laminin physisorbed to plasma-treated (Plasma-Lam) ($n = 10$) surfaces. We calculated mean micropost maximum deflection (δ_{max}) (A), effective frequency (f^*) (B), normalized velocities of contraction ($V_{c}^{*}{}_{max}$) and relaxation ($V_{r}^{*}{}_{max}$) (C), and time between the VR_{max} and VC_{max} peaks (t_{CR}) (D). These measurements were done on the second day after the onset of beating. Micropost deflection curves were obtained for each cell (Figure 1), from which the functional parameters δ_{max}, f^*, $V_{c}^{*}{}_{max}$, $V_{r}^{*}{}_{max}$, and t_{CR} (Figure 3) were calculated. $*p < 0.04$.

contraction (eq 1 in Experimental Section) was higher when laminin was covalently linked to the microposts ($V_{c}^{*}{}_{max}$(GPTMS) = 37.6 ± 5.9 s^{-1}; $V_{c}^{*}{}_{max}$(plasma) = 30.3 ± 1.3 s^{-1}; Figure 4C). We observed no differences in the normalized maximum velocity of relaxation ($V_{r}^{*}{}_{max}$, eq eq 2) (Figure 4C). The time between the maximum relaxation velocity and maximum contraction velocity (t_{CR}, Figure 3) (eq eq 3) marginally decreased when laminin was covalently linked to the microposts (t_{CR}(GPTMS) = 0.09 ± 0.003 s; t_{CR}(plasma) = 0.11 ± 0.02 s; $p < 0.3$; Figure 4D).

3.3. Higher Stability of Laminin Covalent Attachment with APTES[glut] Increases Cell Contractility with Time of Culture. We used APTES[glut]-mediated laminin binding (Supporting Information, Figure S1) as an alternative method to GPTMS-mediated binding to confirm the enhancement in neoCM performance due to covalent attachment of laminin to the functionalized substrate. In this case, we tested isolated neoCMs on microposts with laminin covalently attached via GPTMS or APTES[glut]. On days 1 and 2 after the onset of cell beating, parameters of contractile function were determined for beating neoCMs (Figure 3).

Average values of δ_{max} on days 1 and 2 were higher with microposts with GPTMS[laminin] than with microposts with APTES[glut-laminin] (Figure 5), but differences between averaged samples were not significantly different ($p > 0.05$). On day 1, the average f^* for GPTMS[laminin] microposts was higher than that for APTES[glut-laminin] microposts (Figure 5A). At day 2, f^* decreased for GPTMS[laminin] microposts and increased for APTES[glut-laminin] microposts (Figure 5). Significant differences in f^* between GPTMS[laminin] (decrease) and APTES[glut-laminin]

Figure 5. Contractility parameters of beating neoCMs at days 1 and 2 after the onset of beating on microposts with physisorbed laminin after plasma treatment (Plasma-Lam) ($n = 3$ for day 1 and $n = 2$ for day 2), covalently attached laminin via GPTMS (GPTMS-Lam) ($n = 5$ for day 1 and $n = 11$ for day 2), and laminin covalently attached to gluaraldehyde linked to APTES (APTES-Glut-Lam) ($n = 5$ for day 1 and $n = 10$ for day 2). Micropost deflection curves were obtained for each cell as defined in Figure 3 and Supporting Information, Figure S2, from which δ_{max} (A) and f^* (B) were calculated ($*p < 0.04$). In (A), n.s. = not statistically significant. For (B), ANOVA < 0.05 among populations at days 1 and 2.

(increase) microposts may relate to the level of the surface stability of bonded laminin (Figure 2 and Supporting Information, Figure S7) and organosilane (Supporting Information, Figure S6).

The velocity of contractility increased more with APTES[glut-laminin] functionalization than following GPTMS[laminin] functionalization. Except for $V_{r}^{*}{}_{max}$, all values of $V^{*}{}_{max}$ at day 2 did not differ between GPTMS[laminin] and APTES[glut-laminin] (Figure 6). $V_{c}^{*}{}_{max}$ increased with time for both GPTMS[laminin] and APTES[glut-laminin]. $V_{r}^{*}{}_{max}$ also increased with time in
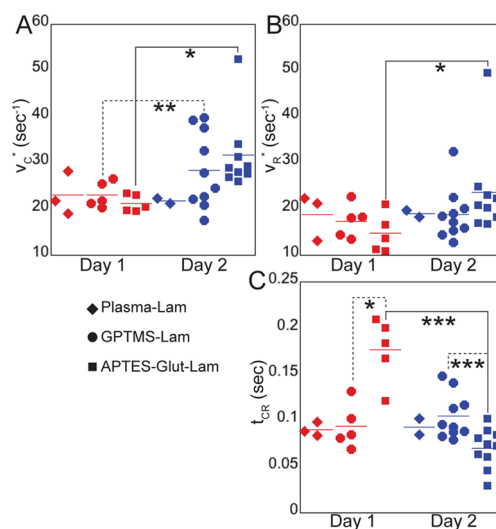
Figure 6. Normalized maximal velocities of contraction ($V_{c}^{*}{}_{max}$) (A) and relaxation ($V_{r}^{*}{}_{max}$) (B) and time between maximal velocity of relaxation and maximal velocity of contraction peaks (t_{CR}) (C) of beating neoCMs at days 1 and 2 after the onset of beating. Cells were attached to microposts with physisorbed laminin after plasma treatment (Plasma-Lam) ($n = 3$ for day 1 and $n = 2$ for day 2), covalently attached laminin via GPTMS (GPTMS-Lam) ($n = 5$ for day 1 and $n = 11$ for day 2) and laminin covalently attached to gluaraldehyde linked to APTES (APTES-Glut-Lam) ($n = 5$ for day 1 and $n = 10$ for day 2). $*p < 0.04$, $**p < 0.05$ calculated with student's t test, $***p < 0.004$. ANOVA p-value for any triad of presented populations >0.05.

APTES[glut-laminin], but did not differ in GPTMS[laminin] between day 1 and day 2. For GPTMS[laminin], t_{CR} did not change. For APTES[glut-laminin], t_{CR} decreased with time. All together, these results suggest that single contractions of neoCMS on APTES[glut-laminin] get faster from day 1 to day 2 (Figure 6). We analyzed smaller samples of neoCMs on microposts with physisorbed laminin (Figures 5 and 6) because we obtained a small amount of contractile cells attached to these microposts.

4. DISCUSSION

4.1. Density and Stability of Covalently Attached Protein Depend on the Surface Properties of PDMS after Functionalization with GPTMS and APTES[glut].

We analyzed protein binding to PDMS to relate contractile phenotypes of neoCMs on microposts to the stability of laminin binding to PDMS. We used laminin-111 (also known as laminin-1)[38] from Engelbreth−Holm−Swarm murine sarcoma basement membrane to culture neoCMs in vitro.[29] We incubated PDMS surfaces with a laminin solution with a concentration of 10 μg/mL, following vendor recommendations to obtain an even coverage of the surface with a laminin monolayer. Different concentrations may result in a different laminin surface distribution and lead to different contractile phenotypes of neoCMs.

Compared to ICC-labeled laminin (Figure 2), a non-homogeneous distribution of gelatin was observed on the tops of the microposts (Supporting Information, Figure S7A). This difference in protein distribution may result from differences between laminin and gelatin properties that mediate intermolecular interactions. Gelatin[39] tends to self-assemble better than laminin-1[40] in these incubation conditions. Fluorescence assays with ICC labeling (Figure 2) of laminin or fluorescently tagged gelatin (Supporting Information, Figure S7) as well as toluidine colorimetric assays (Supporting Information, Figure S5) indicated that double the amount of ligand was present on GPTMS surfaces relative to APTES[glut] surfaces (Supporting Information, Figure S5). However, APTES and APTES[glut-protein] seem to last longer on the surface. These results confirm the differences in protein density observed between ICC labeled laminin on GPTMS and APTES[glut] microposts. More protein is found on GPTMS surfaces than on APTES[glut] surfaces. However, proteins seem to be more stably attached to APTES[glut].

Though time-dependent variations in PDMS surfaces can occur due to continuous surface degradation from the leaching of uncured low molecular weight oligomer siloxanes from the PDMS core into the surface,[37] APTES remained stable on the surface over time in an aqueous environment, suggesting minimal effects from leaching during the incubation time. In contrast, GPTMS surfaces incubated in water chemically changed over 2 d, as revealed by the variations in contact angle ($p < 0.003$) (Supporting Information, Figure S6). Since APTES and GPTMS surface functionalizations are performed in similar conditions, we assume that PDMS oligomer leaching is not the cause of surface changes of GPTMS functionalized PDMS. A portion of proteins on GTPMS is not well attached to the surface (Supporting Information, Figure S7C). Associated with weak binding of a portion of proteins to GPTMS surfaces (Supporting Information, Figure S7C), these surface changes in aqueous environments may also contribute for possible differences in cell adhesion compared to APTES[glut]. These alterations in GPTMS surface chemistry did not occur in anhydrous methanol. The changes of GPTMS surface with water may occur due to the modification of the epoxy group to produce hydroxyl-terminated substrates or due to the rehydration of surfaces and partial removal of silanes from the surface with time.[41] From these results, we conclude that APTES surfaces are more stable than GPTMS. Without silanes, PDMS surfaces are hydrophilic after plasma treatment and undertake a hydrophobic recovery with time due to the release of low molecular weight oligomers from the PDMS core into the surface.[37]

Quantitative measurements of surface properties are summarized in Supporting Information, Table S1. Our procedures for silanization of oxidized PDMS followed previous protocols for the formation of GPTMS and APTES monolayers on silica surfaces;[41] however, our observation of two different ligand densities following GPTMS and APTES[glut] functionalization (Figure 2 and Supporting Information, Figure S7) also suggests that the surface silanization may differ between silica and PDMS. Further, oxidized PDMS surfaces after plasma treatment are different from those of glass and silica.[42] The development of multilayered silane organization or the inhibition of reactive functions[43] may contribute to the generation of different ligand densities. We did not control the orientation of laminin upon binding to surfaces. Therefore, activity of laminin interaction with cells may not be optimal for all laminin molecules throughout functionalized surfaces due to variable conformation and orientation states. The results presented here do not provide information on the conformational state of the laminin molecules on the microposts, on the availability of laminin binding sites, or on interactions of laminins with other laminin neighbors. All of these factors may influence the observed differences in the effects of GPTMS[laminin] and APTES[glut-laminin] functionalizations on neoCM contractility.

4.2. Stronger Binding of Laminin to Microposts Induces neoCMs to Generate Higher Forces.

We hypothesized that the covalent attachment of laminin to the surface of microposts increases the forces generated by neoCMs and that this is due to the increased stability of cell-anchorage sites to the micropost surfaces. NeoCMs were cultured on micropost arrays (Figure 1) with side surfaces separated by 30 μm. Murine neoCMs can be induced to elongate up to 130 μm on flat substrates[44] and thus consistently spanned the 30 μm gap between the microposts. For microposts with physisorbed laminin, cell attachment only occurred when microposts were incubated in laminin solution for a minimum time of 12 h. Surface protein deposition due to physisorption normally occurs within 2−4 h.[45] Our strategy for covalent attachment of laminin with organosilanes takes 3 h and, for this study, is faster than physisorption. Other mechanisms of laminin-surface interaction may be occurring during this process in order for cell attachment to require a minimum incubation time of 12 h. Aldehyde and carbonyl groups that can bind proteins have been identified by others on the surface of plasma-treated PDMS[46] and may covalently bind laminin in solution.

Covalent bonding of extracellular proteins to PDMS enhances cell adhesion and changes biological phenotypes.[17,18] The observed increase in post deflections with GPTMS attachment supports this hypothesis. Covalent attachment of extracellular matrix proteins to PDMS has been shown to increase adhesion, cell spreading area and proliferation of other cell types.[17,18] Increase in cell ligand density[47] and stronger attachments[48] to the extracellular environment lead to higher

force generation. Cytoskeletal changes[18] and mechanisms that regulate the number and density of neoCM adhesion complexes[49] may cause the reported increase in force generation.

Within the myocardium, cardiomyocytes do not build, maintain and rebuild the extracellular matrix. Instead, the structure and composition of the extracellular matrix in the myocardium is remodeled by cardiac fibroblasts,[50] behavior that is also observed *in vitro*.[51] The synthesis of extracellular matrix proteins by neoCMs has never been well determined[52] and we assume it does not occur in this system. Therefore, the presented culture system is not be suitable for long-term cell culture, unless supporting cells are cocultured with neoCMs to remodel the extracellular environment.[50]

Here we present various biomechanical phenotypes of single neoCMs as a function of substrate laminin density. When cultured on top of several microposts, neoCMs exhibit random shapes and contractility occurs isotropically with asynchronous deflection between posts.[10] The contractility of neoCMs immobilized between microposts (Figures 1 and 3 and Supporting Information, Figure S2) resembles the contractility of adult mature cardiomyocytes.[13] As also previously reported relative to other types of cardiomyocytes by Taylor et al.,[9] immobilization of single neoCMs between microposts constrains contractility to occur along the major axis of the cells (Supporting Information, Figure S2). Therefore, the mechanobiology of neoCMs between microposts relative to on top of several microposts[10] may better translate subcellular physiological conditions that affect cardiomyocyte contractility.

4.3. Higher Stability of Laminin Covalent Attachment Increases neoCM Contractility. Why do neoCMs cultured on arrays of microposts functionalized with laminin via GPTMS and APTES[glut] present different biomechanical phenotypes? The observed time-dependent variations in contractile parameters may occur due to biological changes inherent to neoCMs in culture or variations in time of laminin binding stability in the interface between PDMS surfaces and neoCMs. The contractility (beating rate and speeds of contractions), cell size, and calcium signaling of neoCMs in standard culture systems increase with time after isolation.[53−55] The composition of the cell culture media also affects variation in physiological phenotypes in neoCMs *in vitro*.[56] Laminin is incubated without any other proteins in solution and binds the organosilane reactive functions on PDMS surfaces before seeding neoCMs in cell culture media on arrays of microposts. Once covalently attached, laminin should not be replaced by another serum protein, as it occurs in competitive physisorption to surfaces between proteins in solution.[57] However, laminin has binding sites for other matrix proteins and can nonspecifically interact with other serum proteins present in the media.[58] These interactions may affect the adhesion of neoCMs to microposts.

Loss of GPTMS surface stability with time (Supporting Information, Figures S6 and S7) may induce different changes in neoCM contractility relative to APTES[glut] surfaces with more stable laminin adhesion. In addition, laminin functional sites that bind cells contain amino acids with free amines.[59] The binding of these regions to PDMS via organosilanes with amine-binding species may affect the interactions of neoCMs with immobilized laminins. GPTMS and APTES[glut] present different chemical structures that may also differently interact with laminin (Supporting Information, Figure S1B). Proteins interact differently with surfaces of different wettability and net charge, which can affect conformation and activity of proteins on the surfaces with different contact angles as APTES and GPTMS.[60]

Higher laminin density on GPTMS[laminin] microposts induces higher f^* at day 1 (Figure 5). However, loss of laminin with time induces a decrease in f^* at day 2 (Figure 5) and no significant changes in the other contractile phenotypes (Figures 5 and 6). Higher stability of laminin attachment to APTES[glut] microposts induces an increase with time of f^* (Figure 5), $V_c^*{}_{max}$, $V_r^*{}_{max}$, and a decrease in time of t_{CR} (Figure 6). Since we observed that proteins are more stably attached to APTES[glut], our data strongly suggests that changes in the contractile phenotypes of neoCMs when cultured on APTES[glut-laminin] are solely a function of biological changes. Laminin-1 is not abundant in the mature heart. Different neoCM contractile phenotypes may be observed if using laminin isoforms found in a developed heart. However, laminin-1 is strongly involved in heart development[38,61] and is also involved in cardiac regeneration.[62]

4.4. Contractility of neoCMs Cultured on AP-TES[glut-laminin] Microposts Is Similar to What Is Observed under Physiological Conditions. The different variations in contractility between GPTMS[laminin] and APTES[glut-laminin] may be a consequence of different neoCM biological changes known to occur during postnatal development[63] or of different binding mechanism to laminin between GPTMS and APTES[glut]. APTES[glut-laminin] microposts induce improved contractility of neoCMs because the beating rate (f^*), maximum speeds of contraction ($V_c^*{}_{max}$) and relaxation ($V_r^*{}_{max}$) increase with time and times of contractions (t_{CR}) decrease with time (Figures 5 and 6). Homologous changes occur with neoCMs on Petri dishes[53−55] and in postnatal development *in vivo*.[56,63] The speeds of contractility and the beating rates increase, while the times of contraction decrease during *in vivo* postnatal development.[56,63] Replicating variations of *in vivo* phenotypes, the size, contractility, and electrophysiology of neoCMs in culture are known to vary during the first 7 d after isolation.[53−55] When compared to rat neoCMs, the variation of *in vitro* physiological phenotypes of mouse neoCMs is less dependent on serum growth factors,[54] involving an increase with time in the contractility rate,[64] contraction velocities,[65] and a decrease of times of contraction.[65] Such changes are not observed with our microsposts treated with Plasma and GPTMS[laminin]. The higher stability of APTES[glut-laminin]-mediated cell anchorage increases the efficiency of force transfer to posts in the long term, which may lead to the occurrence of *in vivo* contractile phenotypes.

Taken together, our results suggest an increase in maturity of neoCMs attached to APTES[glut-laminin] microposts. Heart disease leads to abnormalities in the force-generation machinery,[66] contractility rate[67] and contraction and relaxation velocities.[68] Size and organization of subcellular sarcomeres relate to neoCM contractile performance[69] and may be differently organized with time in cells on our GPTMS[laminin] and APTES[glut-laminin] micropost surfaces. Cell ligand density on the substrate surface[70] and the extent of cell adhesions can also affect gene expression. Single-cell examinations of gene expression may shed light on the mechanistic pathways controlled by the levels of neoCM adhesion to microposts via laminin with GPTMS or APTES[glut].

5. CONCLUSIONS AND FUTURE WORK

Here, we have demonstrated improved force transduction by contractile neoCMs connected to PDMS microposts following covalent bonding of laminin to PDMS surfaces with organosilanes. GPTMS functionalization resulted in a higher surface density of laminin, while APTES[glut] functionalization yielded the most stable laminin binding to PDMS surfaces. Stability of laminin binding in APTES[glut] microposts leads to an increase with time in neoCM contraction rates ($f*$), to maximum contraction (V_c*_{max}) and relaxation (V_r*_{max}) velocities, and to a decrease in time of times of contraction (t_{CR}). These observations are consistent with the variations in contractility of neoCMs in the first days of *in vitro* culture[53−55] and *in vivo* neonatal development.[56,63] Our data demonstrate a useful way to more carefully control chemical cues and thus better understand mechanical data. Therefore, this strategy for covalently attaching laminin to microposts via APTES[glut] has great potential for the study of the mechanobiological signatures of heart health and disease in single neoCMs. Our PDMS microposts with better tunable and stable surface properties will enable future studies with a variety of extracellular components and will elucidate the interactions of basement-membrane proteins with neoCMs.

■ ASSOCIATED CONTENT

Ⓢ Supporting Information

Supporting images and video of contracting neoCMs. This material is available free of charge via the Internet at http://pubs.acs.org.

■ AUTHOR INFORMATION

Corresponding Author

*E-mail: pruitt@stanford.edu. Fax: +1 650 725 1587. Phone: +1 650 723 2300;

Author Contributions

The manuscript was written through contributions of all authors. All authors have given approval to the final version of the manuscript. A.J.S.R., B.L.P., and E.A.A. designed and initiated this study. K.Z.R. performed cell isolation and provided advice in culture and maintenance of cells. A.J.S.R. fabricated micropost arrays, performed chemical functionalizations, surface characterization, and acquisition and processing of cell contractility data. A.J.S.R. and B.L.P. wrote the manuscript.

Notes

The authors declare no competing financial interest.

■ ACKNOWLEDGMENTS

■ ABBREVIATIONS

NeoCM, mouse neonatal cardiomyocyte
PDMS, polydimethylsiloxane
GPTMS, 3-glycidoxypropyltrimethoxysilane
APTES, 3-aminopropyltriethoxysilane
glut, glutaraldehyde
ICC, immunocytochemistry

■ REFERENCES

(1) Go, A. S.; Mozaffarian, D.; Roger, V. r. L.; Benjamin, E. J.; Berry, J. D.; Borden, W. B.; Bravata, D. M.; Dai, S.; Ford, E. S.; Fox, C. S.; Franco, S.; Fullerton, H. J.; Gillespie, C.; Hailpern, S. M.; Heit, J. A.; Howard, V. J.; Huffman, M. D.; Kissela, B. M.; Kittner, S. J.; Lackland, D. T.; Lichtman, J. H.; Lisabeth, L. D.; Magid, D.; Marcus, G. M.; Marelli, A.; Matchar, D. B.; McGuire, D. K.; Mohler, E. R.; Moy, C. S.; Mussolino, M. E.; Nichol, G.; Paynter, N. P.; Schreiner, P. J.; Sorlie, P. D.; Stein, J.; Turan, T. N.; Virani, S. S.; Wong, N. D.; Woo, D.; Turner, M. B. Heart Disease and Stroke Statistics—2013 Update: A Report from the American Heart Association. *Circulation* **2013**, *127*, e6−e245.
(2) Strobeck, J. E.; Krueger, J.; Sonnenblick, E. H. Load and Time Considerations in the Force-Length Relation of Cardiac Muscle. *Fed. Proc.* **1980**, *39*, 175−182.
(3) Fan, G. C.; Yuan, Q.; Zhao, W.; Chu, G.; Kranias, E. G. Junctin Is a Prominent Regulator of Contractility in Cardiomyocytes. *Biochem. Biophys. Res. Commun.* **2007**, *352*, 617−622.
(4) Iribe, G.; Helmes, M.; Kohl, P. Force-Length Relations in Isolated Intact Cardiomyocytes Subjected to Dynamic Changes in Mechanical Load. *Am. J. Physiol. Heart Circ. Physiol.* **2007**, *292*, H1487−H1497.
(5) Oliveira, S. M.; Zhang, Y. H.; Solis, R. S.; Isackson, H.; Bellahcene, M.; Yavari, A.; Pinter, K.; Davies, J. K.; Ge, Y.; Ashrafian, H.; Walker, J. W.; Carling, D.; Watkins, H.; Casadei, B.; Redwood, C. Amp-Activated Protein Kinase Phosphorylates Cardiac Troponin I and Alters Contractility of Murine Ventricular Myocytes. *Circ. Res.* **2012**, *110*, 1192−1201.
(6) Lockhart, M.; Wirrig, E.; Phelps, A.; Wessels, A. Extracellular Matrix and Heart Development. *Birth Defects Res., Part A* **2011**, *91*, 535−550.
(7) Spinale, F. G.; Zile, M. R. Integrating the Myocardial Matrix into Heart Failure Recognition and Management. *Circ. Res.* **2013**, *113*, 725−738.
(8) Mishra, P. K.; Givvimani, S.; Chavali, V.; Tyagi, S. C. Cardiac Matrix: A Clue for Future Therapy. *Biochim. Biophys. Acta* **2013**, *1832*, 2271−2276.
(9) Taylor, R. E.; Kim, K.; Sun, N.; Park, S. J.; Sim, J. Y.; Fajardo, G.; Bernstein, D.; Wu, J. C.; Pruitt, B. L. Sacrificial Layer Technique for Axial Force Post Assay of Immature Cardiomyocytes. *Biomed. Microdevices* **2013**, *15*, 171−181.
(10) Rodriguez, A. G.; Han, S. J.; Regnier, M.; Sniadecki, N. J. Substrate Stiffness Increases Twitch Power of Neonatal Cardiomyocytes in Correlation with Changes in Myofibril Structure and Intracellular Calcium. *Biophys. J.* **2011**, *101*, 2455−2464.
(11) Domke, J.; Parak, W. J.; George, M.; Gaub, H. E.; Radmacher, M. Mapping the Mechanical Pulse of Single Cardiomyocytes with the Atomic Force Microscope. *Eur. Biophys. J.* **1999**, *28*, 179−186.
(12) Sweitzer, N. K.; Moss, R. L. Determinants of Loaded Shortening Velocity in Single Cardiac Myocytes Permeabilized with Alpha-Hemolysin. *Circ. Res.* **1993**, *73*, 1150−1162.
(13) Louch, W. E.; Sheehan, K. A.; Wolska, B. M. Methods in Cardiomyocyte Isolation, Culture, and Gene Transfer. *J. Mol. Cell. Cardiol.* **2011**, *51*, 288−298.
(14) Bird, S. D.; Doevendans, P. A.; van Rooijen, M. A.; Brutel de la Riviere, A.; Hassink, R. J.; Passier, R.; Mummery, C. L. The Human Adult Cardiomyocyte Phenotype. *Cardiovasc. Res.* **2003**, *58*, 423−434.

(15) McCain, M. L.; Parker, K. K. Mechanotransduction: The Role of Mechanical Stress, Myocyte Shape, and Cytoskeletal Architecture on Cardiac Function. *Pfluegers Arch.* 2011, 462, 89–104.

(16) Schoen, I.; Pruitt, B. L.; Vogel, V. The Yin-Yang of Rigidity Sensing: How Forces and Mechanical Properties Regulate the Cellular Response to Materials. *Annu. Rev. Mater. Res.* 2013, 43, 589–618.

(17) Wipff, P. J.; Majd, H.; Acharya, C.; Buscemi, L.; Meister, J. J.; Hinz, B. The Covalent Attachment of Adhesion Molecules to Silicone Membranes for Cell Stretching Applications. *Biomaterials* 2009, 30, 1781–1789.

(18) Kuddannaya, S.; Chuah, Y. J.; Lee, M. H.; Menon, N. V.; Kang, Y.; Zhang, Y. Surface Chemical Modification of Poly-(Dimethylsiloxane) for the Enhanced Adhesion and Proliferation of Mesenchymal Stem Cells. *ACS Appl. Mater. Interfaces* 2013, 5, 9777–9784.

(19) Rocha-Resende, C.; Roy, A.; Resende, R.; Ladeira, M. S.; Lara, A.; de Morais Gomes, E. R.; Prado, V. F.; Gros, R.; Guatimosim, C.; Prado, M. A.; Guatimosim, S. Non- Neuronal Cholinergic Machinery Present in Cardiomyocytes Offsets Hypertrophic Signals. *J. Mol. Cell. Cardiol.* 2012, 53, 206–216.

(20) Berk, B. C.; Fujiwara, K.; Lehoux, S. Ecm Remodeling in Hypertensive Heart Disease. *J. Clin. Invest.* 2007, 117, 568–575.

(21) Donker, D. W.; Maessen, J. G.; Verheyen, F.; Ramaekers, F. C.; Spatjens, R. L.; Kuijpers, H.; Ramakers, C.; Schiffers, P. M.; Vos, M. A.; Crijns, H. J.; Volders, P. G. Impact of Acute and Enduring Volume Overload on Mechanotransduction and Cytoskeletal Integrity of Canine Left Ventricular Myocardium. *Am. J. Physiol. Heart Circ. Physiol.* 2007, 292, H2324–H2332.

(22) Hein, S.; Schaper, J. The Extracellular Matrix in Normal and Diseased Myocardium. *J. Nucl. Cardiol.* 2001, 8, 188–196.

(23) Colognato, H.; Winkelmann, D. A.; Yurchenco, P. D. Laminin Polymerization Induces a Receptor-Cytoskeleton Network. *J. Cell Biol.* 1999, 145, 619–631.

(24) Dennis, R. G.; Kosnik, P. E., II. Excitability and Isometric Contractile Properties of Mammalian Skeletal Muscle Constructs Engineered in Vitro. *In Vitro Cell. Dev. Biol.: Anim.* 2000, 36, 327–335.

(25) Innocenzi, P.; Kidchob, T.; Yoko, T. Hybrid Organic-Inorganic Sol-Gel Materials Based on Epoxy-Amine Systems. *J. Sol-Gel Sci. Technol.* 2005, 35, 225–235.

(26) Vandenberg, E. T.; Krull, U. J. The Prevention of Adsorption of Interferents to Radiolabelled Protein by Tween 20. *J. Biochem. Biophys. Methods* 1991, 22, 269–277.

(27) Weetall, H. H. Preparation of Immobilized Proteins Covalently Coupled through Silane Coupling Agents to Inorganic Supports. *Appl. Biochem. Biotechnol.* 1993, 41, 157–188.

(28) Toworfe, G. K.; Bhattacharyya, S.; Composto, R. J.; Adams, C. S.; Shapiro, I. M.; Ducheyne, P. Effect of Functional End Groups of Silane Self-Assembled Monolayer Surfaces on Apatite Formation, Fibronectin Adsorption and Osteoblast Cell Function. *J. Tissue Eng. Regener. Med.* 2009, 3, 26–36.

(29) Devic, E.; Xiang, Y.; Gould, D.; Kobilka, B. Beta-Adrenergic Receptor Subtype- Specific Signaling in Cardiac Myocytes from Beta(1) and Beta(2) Adrenoceptor Knockout Mice. *Mol. Pharmacol.* 2001, 60, 577–583.

(30) Kuhn, J. R.; Poenie, M. Dynamic Polarization of the Microtubule Cytoskeleton During Ctl-Mediated Killing. *Immunity* 2002, 16, 111–121.

(31) Wu, Y.; Hussain, M.; Fassihi, R. Development of a Simple Analytical Methodology for Determination of Glucosamine Release from Modified Release Matrix Tablets. *J. Pharm. Biomed. Anal.* 2005, 38, 263–269.

(32) Abass, A. K. Study the Effects Influencing the Adsorption of Toluidine Blue O (Tbo) Dye onto Mno2 Surface. *Iraqi Natl. J. Chem.* 2008, 306–322.

(33) Dancey, C.; Reidy, J.; Rowe, R. *Statistics for the Health Sciences: A Non-Mathematical Introduction*; SAGE Publications: Thousand Oaks, CA, 2012; Chapter 7, pp 237–240.

(34) Ramos-Vara, J. A. Technical Aspects of Immunohistochemistry. *Vet. Pathol.* 2005, 42, 405–426.

(35) Chen, X.; Cui, D.; Li, H.; Cai, H.; Sun, J.; Chen, J. Microfluidics-Based Immunoassays by Using an Integrated Fluorescence Detection System. *Microsyst. Technol.* 2010, 16, 2049–2055.

(36) Lee, M. H.; Brass, D. A.; Morris, R.; Composto, R. J.; Ducheyne, P. The Effect of Non- Specific Interactions on Cellular Adhesion Using Model Surfaces. *Biomaterials* 2005, 26, 1721–1730.

(37) Lee, D.; Yang, S. Surface Modification of Pdms by Atmospheric-Pressure Plasma- Enhanced Chemical Vapor Deposition and Analysis of Long-Lasting Surface Hydrophilicity. *Sens. Actuators, B* 2012, 162, 425–434.

(38) Ekblom, P.; Lonai, P.; Talts, J. F. Expression and Biological Role of Laminin-1. *Matrix Biol.* 2003, 22, 35–47.

(39) Mohanty, B.; Bohidar, H. B. Systematic of Alcohol-Induced Simple Coacervation in Aqueous Gelatin Solutions. *Biomacromolecules* 2003, 4, 1080–1086.

(40) Cheng, Y. S.; Champliaud, M. F.; Burgeson, R. E.; Marinkovich, M. P.; Yurchenco, P. D. Self-Assembly of Laminin Isoforms. *J. Biol. Chem.* 1997, 272, 31525–31532.

(41) Lee, M. H.; Boettiger, D.; Ducheyne, P.; Composto, R. J. Self-Assembled Monolayers of Omega-Functional Silanes: A Platform for Understanding Cellular Adhesion at the Molecular Level. In *Silanes and Other Coupling Agents,* Vol. 4; Mittal, K. L., Ed.; CRC Press, Taylor & Francis Group, LLC: Boca Raton, FL, 2007; Part 1, pp 163–178.

(42) Zhou, J.; Ellis, A. V.; Voelcker, N. H. Recent Developments in PDMS Surface Modification for Microfluidic Devices. *Electrophoresis* 2010, 31, 2–16.

(43) Wang, A.; Tang, H.; Cao, T.; Salley, S. O.; Ng, K. Y. In Vitro Stability Study of Organosilane Self-Assemble Monolayers and Multilayers. *J. Colloid Interface Sci.* 2005, 291, 438–447.

(44) Bray, M. A.; Sheehy, S. P.; Parker, K. K. Sarcomere Alignment Is Regulated by Myocyte Shape. *Cell Motil. Cytoskeleton* 2008, 65, 641–651.

(45) Ruggiero, C.; Mantelli, M.; Curtis, A.; Zhang, S.; Rolfe, P. Computer Modelling of the Adsorption of Proteins on Solid Surfaces under the Influence of Double Layer and Van Der Waals Energy. *Med. Biol. Eng. Comput.* 1999, 37, 119–124.

(46) Williams, R. L.; Wilson, D. J.; Rhodes, N. P. Stability of Plasma-Treated Silicone Rubber and Its Influence on the Interfacial Aspects of Blood Compatibility. *Biomaterials* 2004, 25, 4659–4673.

(47) Koo, L. Y.; Irvine, D. J.; Mayes, A. M.; Lauffenburger, D. A.; Griffith, L. G. Co-Regulation of Cell Adhesion by Nanoscale RGD Organization and Mechanical Stimulus. *J. Cell Sci.* 2002, 115, 1423–1433.

(48) Zielinski, R.; Mihai, C.; Kniss, D.; Ghadiali, S. N. Finite Element Analysis of Traction Force Microscopy: Influence of Cell Mechanics, Adhesion, and Morphology. *J. Biomech. Eng.* 2013, 135, 71009.

(49) Gad, A. K.; Ronnlund, D.; Spaar, A.; Savchenko, A. A.; Petranyi, G.; Blom, H.; Szekely, L.; Widengren, J.; Aspenstrom, P. Rho GTPases Link Cellular Contractile Force to the Density and Distribution of Nanoscale Adhesions. *FASEB J.* 2012, 26, 2374–2382.

(50) Khan, R.; Sheppard, R. Fibrosis in Heart Disease: Understanding the Role of Transforming Growth Factor-Beta in Cardiomyopathy, Valvular Disease and Arrhythmia. *Immunology* 2006, 118, 10–24.

(51) LaFramboise, W. A.; Scalise, D.; Stoodley, P.; Graner, S. R.; Guthrie, R. D.; Magovern, J. A.; Becich, M. J. Cardiac Fibroblasts Influence Cardiomyocyte Phenotype in Vitro. *Am. J. Physiol.: Cell Physiol.* 2007, 292, C1799–1808.

(52) Stastna, M.; Chimenti, I.; Marban, E.; Van Eyk, J. E. Identification and Functionality of Proteomes Secreted by Rat Cardiac Stem Cells and Neonatal Cardiomyocytes. *Proteomics* 2010, 10, 245–253.

(53) Simpson, P.; McGrath, A.; Savion, S. Myocyte Hypertrophy in Neonatal Rat Heart Cultures and Its Regulation by Serum and by Catecholamines. *Circ. Res.* 1982, 51, 787–801.

(54) Deng, X. F.; Rokosh, D. G.; Simpson, P. C. Autonomous and Growth Factor-Induced Hypertrophy in Cultured Neonatal Mouse Cardiac Myocytes. Comparison with Rat. *Circ. Res.* 2000, 87, 781–788.

(55) Husse, B.; Wussling, M. Developmental Changes of Calcium Transients and Contractility During the Cultivation of Rat Neonatal Cardiomyocytes. *Mol. Cell. Biochem.* **1996**, *163−164*, 13−21.

(56) Gomez, J. P.; Potreau, D.; Branka, J. E.; Raymond, G. Developmental Changes in Ca^{2+} Currents from Newborn Rat Cardiomyocytes in Primary Culture. *Pfluegers Arch.* **1994**, *428*, 241−249.

(57) Roa Romero, L. M.; Felgueiras, H.; Migonney, V.; Sommerfeld, S.; Murthy, N. S.; Kohn, J., Competitive Adsorption of Albumin, Fibronectin and Collagen Type I on Different Biomaterial Surfaces: A Qcm-D Study. In *XIII Mediterranean Conference on Medical and Biological Engineering and Computing 2013;* Springer International Publishing: New York, 2013; pp 1597−1600.

(58) Hohenester, E.; Engel, J. Domain Structure and Organisation in Extracellular Matrix Proteins. *Matrix Biol.* **2002**, *21*, 115−128.

(59) Graf, J.; Iwamoto, Y.; Sasaki, M.; Martin, G. R.; Kleinman, H. K.; Robey, F. A.; Yamada, Y. Identification of an Amino Acid Sequence in Laminin Mediating Cell Attachment, Chemotaxis, and Receptor Binding. *Cell* **1987**, *48*, 989−996.

(60) Anand, G.; Sharma, S.; Dutta, A. K.; Kumar, S. K.; Belfort, G. Conformational Transitions of Adsorbed Proteins on Surfaces of Varying Polarity. *Langmuir* **2010**, *26*, 10803−10811.

(61) De Arcangelis, A.; Neuville, P.; Boukamel, R.; Lefebvre, O.; Kedinger, M.; Simon- Assmann, P. Inhibition of Laminin Alpha 1-Chain Expression Leads to Alteration of Basement Membrane Assembly and Cell Differentiation. *J. Cell Biol.* **1996**, *133*, 417−430.

(62) Castaldo, C.; Di Meglio, F.; Nurzynska, D.; Romano, G.; Maiello, C.; Bancone, C.; Muller, P.; Bohm, M.; Cotrufo, M.; Montagnani, S. Cd117-Positive Cells in Adult Human Heart Are Localized in the Subepicardium, and Their Activation Is Associated with Laminin-1 and Alpha6 Integrin Expression. *Stem Cells* **2008**, *26*, 1723−1731.

(63) Adachi, T.; Shibata, S.; Okamoto, Y.; Sato, S.; Fujisawa, S.; Ohba, T.; Ono, K. The Mechanism of Increased Postnatal Heart Rate and Sinoatrial Node Pacemaker Activity in Mice. *J. Physiol. Sci.* **2013**, *63*, 133−146.

(64) Luyken, J.; Hannan, R. D.; Cheung, J. Y.; Rothblum, L. I. Regulation of Rdna Transcription During Endothelin-1-Induced Hypertrophy of Neonatal Cardiomyocytes. Hyperphosphorylation of Upstream Binding Factor, an Rdna Transcription Factor. *Circ. Res.* **1996**, *78*, 354−361.

(65) Hill, C.; Wurfel, A.; Heger, J.; Meyering, B.; Schluter, K. D.; Weber, M.; Ferdinandy, P.; Aronheim, A.; Schulz, R.; Euler, G. Inhibition of Ap-1 Signaling by Jdp2 Overexpression Protects Cardiomyocytes against Hypertrophy and Apoptosis Induction. *Cardiovasc. Res.* **2013**, *99*, 121−128.

(66) Sharov, V. G.; Sabbah, H. N.; Shimoyama, H.; Ali, A. S.; Levine, T. B.; Lesch, M.; Goldstein, S. Abnormalities of Contractile Structures in Viable Myocytes of the Failing Heart. *Int. J. Cardiol.* **1994**, *43*, 287−297.

(67) Hamrell, B. B.; Alpert, N. R. The Mechanical Characteristics of Hypertrophied Rabbit Cardiac Muscle in the Absence of Congestive Heart Failure: The Contractile and Series Elastic Elements. *Circ. Res.* **1977**, *40*, 20−25.

(68) Wang, Q.; Moncman, C. L.; Winkelmann, D. A. Mutations in the Motor Domain Modulate Myosin Activity and Myofibril Organization. *J. Cell Sci.* **2003**, *116*, 4227−4238.

(69) Kuo, P. L.; Lee, H.; Bray, M. A.; Geisse, N. A.; Huang, Y. T.; Adams, W. J.; Sheehy, S. P.; Parker, K. K. Myocyte Shape Regulates Lateral Registry of Sarcomeres and Contractility. *Am. J. Pathol.* **2012**, *181*, 2030−2037.

(70) Trappmann, B.; Gautrot, J. E.; Connelly, J. T.; Strange, D. G.; Li, Y.; Oyen, M. L.; Cohen Stuart, M. A.; Boehm, H.; Li, B.; Vogel, V.; Spatz, J. P.; Watt, F. M.; Huck, W. T. Extracellular-Matrix Tethering Regulates Stem-Cell Fate. *Nat. Mater.* **2012**, *11*, 642−649.